01 May 2006

Benchmarking High-Field Few-Electron Correlation and QED Contributions in Hg^{75+} to Hg^{78+} Ions. I. Experiment

Antonio J. Gonzalez

Jose R. Crespo Lopez-Urrutia

Jean Pierre Braun

Gunter Brenner

et. al. For a complete list of authors, see https://scholarsmine.mst.edu/phys_facwork/827

Recommended Citation

A. J. Gonzalez and J. R. Crespo Lopez-Urrutia and J. P. Braun and G. Brenner and H. Bruhns and A. Lapierre and V. S. Mironov and R. Soria Orts and H. Tawara and M. Trinczek and J. H. Ullrich and A. N. Artemyev and Z. Harman and U. D. Jentschura and C. H. Keitel and J. H. Scofield and I. I. Tupitsyn, "Benchmarking High-Field Few-Electron Correlation and QED Contributions in Hg^{75+} to Hg^{78+} Ions. I. Experiment," *Physical Review A - Atomic, Molecular, and Optical Physics*, vol. 73, no. 5, pp. 052710-1-052710-10, American Physical Society (APS), May 2006.
The definitive version is available at https://doi.org/10.1103/PhysRevA.73.052710

Benchmarking high-field few-electron correlation and QED contributions in Hg^{75+} to Hg^{78+} ions. I. Experiment

A. J. González Martínez,[1] J. R. Crespo López-Urrutia,[1] J. Braun,[1] G. Brenner,[1] H. Bruhns,[1] A. Lapierre,[1] V. Mironov,[1] R. Soria Orts,[1] H. Tawara,[1] M. Trinczek,[1] J. Ullrich,[1] A. N. Artemyev,[2] Z. Harman,[1] U. D. Jentschura,[1] C. H. Keitel,[1] J. H. Scofield,[3] and I. I. Tupitsyn[2]

[1]*Max-Planck-Institut für Kernphysik, D-69117 Heidelberg, Germany*

[2]*St. Petersburg State University, St. Petersburg 198504, Russia*

[3]*Lawrence Livermore National Laboratory, Livermore, California 94550, USA*

(Received 6 December 2005; published 23 May 2006)

The photorecombination of highly charged few-electron mercury ions Hg^{75+} to Hg^{78+} has been explored with the Heidelberg electron beam ion trap. By monitoring the emitted x rays (65–76 keV) and scanning the electron beam energy (45–54 keV) over the *KLL* dielectronic recombination (DR) region, the energies of state-selected DR resonances were determined to within ±4 eV (relative) and ±14 eV (absolute). At this level of experimental accuracy, it becomes possible to make a detailed comparison to various theoretical approaches and methods, all of which include quantum electrodynamic (QED) effects and finite nuclear size contributions (for a $1s$ electron, these effects can be as large as 160 and 50 eV, respectively). In He-like Hg^{78+}, a good agreement between the experimental results and the calculations has been found. However, for the capture into Li-, Be-, and B-like ions, significant discrepancies have been observed for specific levels. The discrepancies suggest the need for further theoretical and experimental studies with other heavy ions along these isoelectronic sequences.

DOI: 10.1103/PhysRevA.73.052710 PACS number(s): 34.80.Lx, 32.80.Hd, 52.25.Os

I. INTRODUCTION

During the last two decades, increasingly accurate measurements of transition energies and probabilities, electron-impact excitation, and ionization cross sections in highly charged ions (HCIs) have significantly improved our understanding of contributions due to relativity, quantum electrodynamics (QED), finite nuclear size, and electronic correlations (for review article see, e.g., Refs. [1–3]). Apart from the last one, their relative importance, compared to the predictions of the Schrödinger equation, increases tremendously with high powers of the nuclear charge Z, i.e., with growing strength of the confining electromagnetic fields. Thus, approaching high fields of up to 10^{19} V/cm and 10^8 T close to the nucleus—the strongest ones to be realized in earthbound laboratories—and, at the same time, controlling the contribution of electronic correlation effects by involving a well-defined and small number of electrons, HCIs are the most attractive systems to benchmark state-of-the-art relativistic and QED atomic structure theories.

Highly charged ions with less than five bound electrons and a nuclear charge number exceeding $Z \geqslant 80$ represent especially demanding systems for theory. A number of otherwise negligibly small contributions have to be taken into account. Among them are relativistic modifications of the electron-electron interactions, contributions of higher orders in the perturbation expansion in the parameter $Z\alpha$ of the electron self-energy and of the vacuum polarization, as well as effects due to the finite nuclear size (here, α is the fine-structure constant). Moreover, and extremely challenging, some of them are intimately intertwined with each other not only in view of a unified theoretical description of relativity and quantum field theory but, in particular, due to the fact that their absolute magnitudes, scaling with different powers of Z, become similar and cannot be treated independently, demanding for theory development towards the limits of our present understanding. For example, the binding energies of the $1s2s^2$ doubly excited levels of Li-like Hg^{77+} ($Z=80$) contains relativistic and nonrelativistic correlation contributions of the same order of magnitude (−17 and −37 eV, respectively), while the finite nuclear size affects the $1s^2$ ground state energy of He-like Hg^{78+} with a contribution as large as 108 eV. At the same time, QED effects become important both in the ground and excited states, reaching magnitudes of about 300 and 200 eV, respectively.

Despite their fundamental importance and increasing research activities, there exist only a few measurements of electronic transitions involving HCIs of less than five electrons and nuclear charge numbers exceeding $Z=80$. This shortage of precise data for few-electron heavy ions results mainly from the difficulties of producing them in sufficient numbers and of reaching a high level of statistical significance in the data. As their electrons are tightly bound to the nucleus (the binding energy is ≈132 keV for U^{91+} ions), accelerators were used from early on to reach the ion energies (sometimes >100 MeV/u, $v/c \approx 0.5$) required to strip most of their electrons off by beam foil methods. Despite these experimental challenges, the $2s_{1/2}$-$2p_{1/2}$ transition energy in Li-like U^{89+} ions, for example, has been determined with an accuracy of 400 ppm after correcting for the satellite electron and Doppler effects inherent to such ion beam-foil techniques [4]. Enabled by the development of heavy-ion-storage rings about 10 years ago, a similar accuracy has been reached through studies of dielectronic resonances into high Rydberg states at the GSI experimental storage ring (ESR) in Darmstadt for the same transition in Li-like Au, Pb, and U

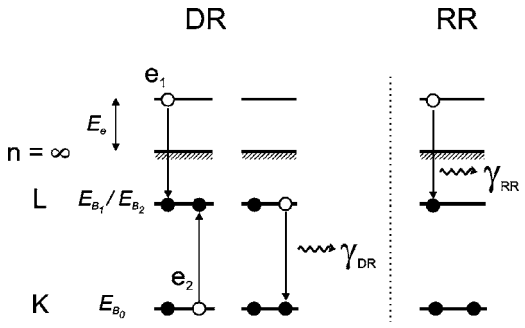

FIG. 1. Sketch of the dielectronic (DR) and radiative recombination (RR) processes of He-like ions (initial state) in collisions with free electrons.

(see Ref. [5]). Also, the $1s$ Lamb shift in H-like U^{91+} has recently been determined with an uncertainty of ±4.6 eV, corresponding to ≈35 ppm, through precision measurements of $K\alpha_1$ lines after radiative recombination into the $2p_{3/2}$ level of bare U^{92+} at the ESR [6]. In contrast to accelerators, the more compact electron beam ion traps (EBIT) produce a high density of HCIs by means of an energetic electron beam and have made possible precision measurements for the heaviest ions with well-defined charge states without satellite electrons (satellite-electron-free) and with minimum Doppler effects (hundreds of eV). So far, the most accurate measurements of the $2s_{1/2}$-$2p_{3/2}$ transition energy of ≈4.5 keV in few-electron U^{89+} to U^{82+} have been performed with uncertainties of approximately 37 ppm using a crystal spectrometer [7]. A similar technique has been applied to Li-like Bi^{80+} to measure the energy of the same transition with a slightly better accuracy of 14 ppm. The resolving power reached in this experiment also allowed us to determine the hyperfine splitting of the $2s$ ground state [8]. Very recently, a new measurement of the $2s_{1/2}$-$2p_{1/2}$ transition in Li-like U^{89+} has been reported by Beiersdorfer [9], with a value of 280.645(15) eV, reaching a 50 ppm accuracy. The error corresponds to only 7% of the 0.22 eV two-loop contribution to the Lamb shift of the $2s$ electron.

However, most of these previous experimental studies in few-electron HCIs of $Z>80$ dealt with singly excited states for which the electronic correlation can be of minor importance. In contrast, doubly excited states in such ions are more challenging for theory because of their strong coupling to a continuum electron and their open inner shells, which enhance the effect of electron correlation. In this paper, we present accurate measurements of dielectronic recombination resonance energies in doubly excited $2l2l'$ levels of few-electron Hg^{78+} to Hg^{75+} ions performed at an EBIT. We compare these measurements to the results of advanced theoretical calculations including relativistic correlation and QED effects.

Dielectronic recombination (DR) is a resonant process (see Fig. 1) where a free electron (e_1) is captured by an ion into an excited state of binding energy E_{B_1} and a bound electron (e_2, initially in a state with binding energy E_{B_0}) is simultaneously excited into another state of binding energy E_{B_2} (here, all binding energies are counted as non-negative quantities). Later, this intermediate excited state deexcites either through electron (Auger decay) or by photon emission. However, for heavy, highly charged ions, photon emission is more likely, producing a photon of well-defined energy of either $E_{\gamma_{\mathrm{DR}}}=E_{B_0}-E_{B_1}$ or $E_{\gamma_{\mathrm{DR}}}=E_{B_0}-E_{B_2}$. Occurring resonantly, the incident electron energy E_e plus the binding energy E_{B_1} of the recombining state is equal to the excitation energy E_{B_2} of the intermediate doubly excited state (or multi-excited) such that $E_e+E_{B_1}=E_{B_0}-E_{B_2}$ (see the bright spots in Fig. 2).

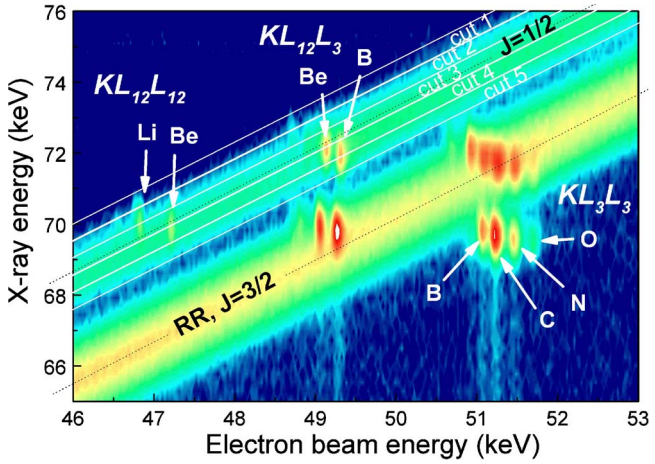

FIG. 2. (Color online) Logarithmic 2D contour-map (x-ray counts as a function of electron energy and x-ray energy) of photorecombination of highly charged mercury ions showing *KLL* DR resonances, which appear as bright spots at particular electron energies (*KLL*: promotion of a bound K shell electron to an L shell and simultaneous capture of a free electron into another L shell). The two continuous diagonal bands correspond to x rays due to RR processes into $J=1/2$ (upper) and $J=3/2$ (lower) levels of the L shell, respectively.

In contrast, radiative recombination (RR) takes place at any electron energy when a free electron is captured into a vacant state E_{B_1} of an ion, releasing the excess energy as a photon. Thus, the energy of the emitted photon $E_{\gamma_{\mathrm{RR}}}$ increases linearly with the electron energy E_e: $E_{\gamma_{\mathrm{RR}}}=E_e+E_{B_1}$ (diagonal bands in Fig. 2 with a slope of unity). At electron energies equal to the DR resonance energies, as the initial and final states are the same in DR and RR, both pathways are indistinguishable and, as a result, quantum interference can occur [10,11].

Note that in this paper we classify the recombination resonances according to the initial state of the ion in the recombination process such as He-, Li-, Be-, or B-like ion systems. An example is shown in Fig. 1 (He-like ion).

This paper is organized as follows: in Sec. II we briefly describe the different theoretical methods used for the comparison to the experimental data. In Sec. III we describe the experimental setup. In Sec. IV we discuss the DR energy spectra, the determination of the DR resonance energies, as well as their differences. Section V is dedicated to the results of the DR x-ray photon energy. This leads to conclusions and forthcoming perspectives in Sec. VI.

II. THEORETICAL METHODS

In the following, short summaries of the theoretical methods used are given.

TABLE I. Measured and theoretical DR resonance energies (keV) of the intermediate excited states $[d]_J$ of He-, Li-, Be-, and B-like mercury ions. The $MCDF_S$ He_1 resonance energy is used as reference for the energy scale (see text). The $(1s2s)_0 2p_{3/2}$, $J=3/2$ level of Li-like ions and $1s2s^2(2p_{1/2})^2 2p_{3/2}$, $J=1$ level of C-like ions have two radiative decay channels which are designated with two different labels, He_3, and He_5, and B_1 and B_3, respectively. We recall that all DR resonances are specified according to the initial charge state of the ion (before recombination). For an explanation of the acronyms used for the theoretical methods applied see Sec. II.

$[d]_J$	Label	Experiment	$MCDF_S$	CI-DFS	QMB	$MCDF_M$
$[1s2s^2]_{1/2}$	He_1	46.358(4)	46.358	46.361	46.359	46.362
$[(1s2s)_0 2p_{1/2}]_{1/2}$	He_2	46.611(6)	46.613	46.614	46.612	46.614
$[(1s2s)_0 2p_{3/2}]_{3/2}$	He_3	48.844(6)	48.844	48.843	48.840	48.842
$[(1s2p_{1/2})_0 2p_{3/2}]_{3/2}$	He_4	48.918(9)	48.923	48.926	48.922	48.926
$[(1s2s)_0 2p_{3/2}]_{3/2}$	He_5	48.845(5)	48.844	48.843	48.840	48.842
$[1s(2p_{3/2})_2^2]_{5/2}$	He_6	51.064(6)	51.065	51.064	51.058	51.065
$[1s2s^2 2p_{1/2}]_1$	Li_1	46.686(5)	46.688	46.690	46.686	46.688
$[((1s2s)_1 2p_{1/2})_{3/2} 2p_{3/2}]_2$	Li_2	49.086(6)	49.066	49.067	49.063	49.077
$[((1s2s)_1 2p_{1/2})_{3/2} 2p_{3/2}]_1$	Li_3	49.136(9)	49.116	49.118	49.113	49.126
$[((1s2s)_0 2p_{1/2})_{1/2} 2p_{3/2}]_2$	Li_4	49.218(13)	49.212	49.214	49.209	49.215
$[((1s2s)_1 2p_{1/2})_{3/2} 2p_{3/2}]_3$	Li_5	48.970(5)	48.964	48.966	48.961	48.971
$[(1s2s)_1 (2p_{3/2})_2^2]_3$	Li_6	51.154(5)	51.150	51.153	51.147	51.155
$[1s2s^2(2p_{1/2})^2]_{1/2}$	Be_1	47.135(5)	47.124	47.135	47.121	47.134
$[(1s2s^2 2p_{1/2})_1 2p_{3/2}]_{3/2}$	Be_2	49.270(8)	49.248	49.260	49.251	49.260
$[(1s2s^2 2p_{1/2})_0 2p_{3/2}]_{3/2}$	Be_3	49.349(6)	49.335	49.347	49.333	49.346
$[(1s2s^2 2p_{1/2})_1 2p_{3/2}]_{5/2}$	Be_4	49.265(17)	49.244	49.254	49.246	49.253
$[1s2s^2(2p_{3/2})_2^2]_{5/2}$	Be_5	51.433(6)	51.425	51.429	51.423	51.430
$[1s2s^2(2p_{1/2})^2 2p_{3/2}]_1$	B_1	49.557(4)	49.549	49.551	49.546	49.553
$[1s2s^2(2p_{1/2})^2 2p_{3/2}]_2$	B_2	49.499(4)	49.491	49.493	49.487	49.493
$[1s2s^2(2p_{1/2})^2 2p_{3/2}]_1$	B_3	49.552(7)	49.549	49.551	49.546	49.553
$[(1s2s^2 2p_{1/2})_1 (2p_{3/2})_2^2]_3$	B_4	51.603(8)	51.601	51.603	51.593	51.598

(*a*) Predictions obtained by the multiconfiguration Dirac-Fock method with the average level (AL) scheme are labeled throughout by $MCDF_S$. The atomic many-electron state function is given as a linear combination of configuration state functions (CSFs) of the same total angular momentum and parity quantum numbers. In the AL calculations, the orbital wave functions are obtained by minimizing the statistically averaged energy of all the involved levels. Quantum electrodynamic corrections are included in an approximate way. The $MCDF_S$ method is described in more detail in [11,12] and references therein.

(*b*) The second set of predictions was performed by using a Dirac-Hartree-Fock (DF) basis set for occupied states and a Dirac-Fock-Sturm (DF-Sturm) basis for the unoccupied ones (configuration interaction, CI-DFS). Here, the wave function sets were generated including all of the single, double, and most triple electronic excitations to the main configuration. The Breit electron-electron interaction (in the Coulomb gauge), the nuclear size (field shift), and QED corrections were all included in the Hamiltonian. More details on this method will be presented in [13].

(*c*) Predictions based on quantum electrodynamic many-body theory are given in the column labeled QMB in Table I. Up to now they have been successfully applied to the calculations of the low-lying levels of highly charged ions with one to three electrons (see, e.g., [14] and references therein). In zeroth-order approximation, only the interaction of the electrons with the nucleus is included. In first order, electron-electron interaction is described by the one-photon exchange diagram using the full photon propagator. The one-electron self-energy and vacuum-polarization (VP) corrections are taken into account. The self-energy screening and vacuum-polarization screening terms largely cancel out and are thus neglected in this approach. Two-photon exchange diagrams are calculated in the relativistic many-body perturbation theory (RMBPT) approximation, as it has been shown that the results obtained in this way differ only in the order of 0.5 eV, from full QED calculations [15].

(*d*) Multiconfiguration Dirac-Fock optimal level (OL) results are labeled by $MCDF_M$. (Here, the subindex *M* indicates the Max-Planck-Institute.) In the case of the OL scheme, the energy functional of a chosen electronic state is minimized. Here, separate OL calculations for each of the ground and excited states involved in the DR process are performed using the GRASP92 implementation of the MCDF method [16]. Correlation configurations correspond-

ing to single and double virtual excitations from occupied states have been applied. This configuration set is systematically extended to analyze the convergence of the configuration expansion and to estimate the accuracy of the self-consistent calculations. Electronic correlation effects due to the frequency-independent Breit interaction and to the normal and specific mass shift are accounted for by a relativistic configuration interaction procedure. The frequency dependence of the Breit retardation operator was included as a first-order perturbation. One-electron vacuum-polarization and self-energy corrections are included exactly and improved approximate methods are utilized to account for electron screening effects. These calculations are described in detail in the companion paper [13].

III. EXPERIMENT

The present measurements have been carried out in the Heidelberg EBIT at the Max-Planck-Institut für Kernphysik [17], using an experimental setup already described in detail in Refs. [10,18,19]. Shortly, in an EBIT, an electron beam is accelerated towards the ionization/trapping region where it is strongly compressed by a magnetic field (8 T in our case) produced by a pair of superconducting coils. This results in highly efficient ionization of ions through successive collisions and, at the same time, produces a deep negative space charge potential radially trapping the produced ions. In order to confine the ions in the longitudinal direction, a set of independently biased drift tubes is used.

Mercury atoms from an evaporating sample were injected into the trap region as a differentially pumped atomic beam. The electron beam current I_e was fixed at 160 mA while the electron beam energy E_e was scanned at a slow rate of about 37 V/s from 45 to 54 keV over a series of *KLL* resonances of various charge states (see Fig. 2). This voltage scan is kept slow in order to maintain a nearly steady-state equilibrium between the ionization and recombination rates. A high axial trapping potential of +2.5 kV was applied to the drift tubes next to the trap center in order to accumulate heavy mercury ions more efficiently.

The electron beam energy is defined by the potential difference between the electron gun and the central drift tube. The electron gun cathode was biased at a constant voltage of -1501.5 ± 0.1 V. The gun itself was installed on a high-voltage platform to which a variable potential of $\approx-(34-43)$ kV was applied. Its value was determined by means of a high-precision voltage divider with a ratio of 39980.5 ± 1.5. A second voltage divider was used to measure the voltage applied to the drift tubes (constant at $\approx+10$ kV). The output voltages of both dividers were recorded every 200 ms. The low scanning rate of the electron acceleration voltage was also critical to minimize the time lag between the applied voltage and its reading through the dividers. The space charge of the electron beam affects the beam energy in a noticeable way as we will explain below.

The x-ray photons emitted from the trapped ions were detected with a high-purity germanium detector, which had an energy resolution of about 700 eV at 75 keV. This detector was calibrated every 4 h during data accumulation through the Kα and Kβ lines of tungsten, tantalum, and lead, excited by 122 keV gamma rays from a ^{57}Co source, thus covering the whole energy range of the DR resonances under study.

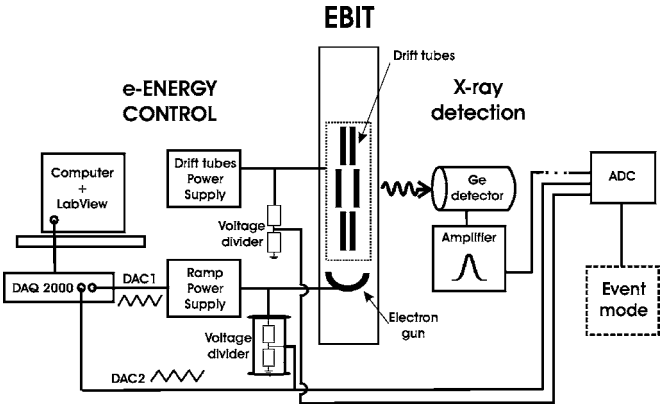

FIG. 3. Overall scheme of the data acquisition system.

The output voltage of the platform divider was fed into one of the channels of an event-mode data acquisition system. A second channel recorded the energy of each photon. Thus, each event consists of (*i*) electron energy through two acceleration voltages reading, (*ii*) photon energy, and (*iii*) time. In order to establish the acceleration voltage scale, the high-accuracy data continuously recorded by means of a GPIB-interfaced personal computer were assigned to the event-mode data scanning range (see Fig. 3).

IV. ELECTRON ENERGY

A. Dielectronic recombination spectra

Figure 2 displays a typical 2D contour map (electron energy against x-ray energy) of the ion-electron recombination processes observed in the *KLL* region. The two diagonal bands arise from x rays emitted during RR into $n=2$ levels with total angular momentum $J=1/2$ (upper band) and $J=3/2$ (lower band). The DR resonances appear in this figure in five distinct groups at different electron energies depending on J. The region of the lowest electron energy corresponds to the DR peaks where both active electrons (the promoted and the captured one) occupy $J=1/2$ levels (denoted as $KL_{12}L_{12}$ in Fig. 2). Those in the intermediate region correspond to excitation and capture into $J=1/2$ and $J=3/2$ levels, and at the highest electron energy for both active electrons going into $J=3/2$ levels are distinguishable (denoted as $KL_{12}L_3$ and KL_3L_3, respectively, in Fig. 2).

Some other x-ray features, seen in Fig. 2 as vertical lines "falling down" from some DR resonances, have broad x-ray energy distributions at well-defined electron energies. They are due to two-photon decay channels [20]. These transitions are very interesting by themselves. However, they were not the focus of our present experimental investigation, and also no precise theoretical predictions for many-electron ions are available [21,22].

Projections of narrow slices cut out along the diagonal RR bands onto the electron beam energy axis (see the areas en-

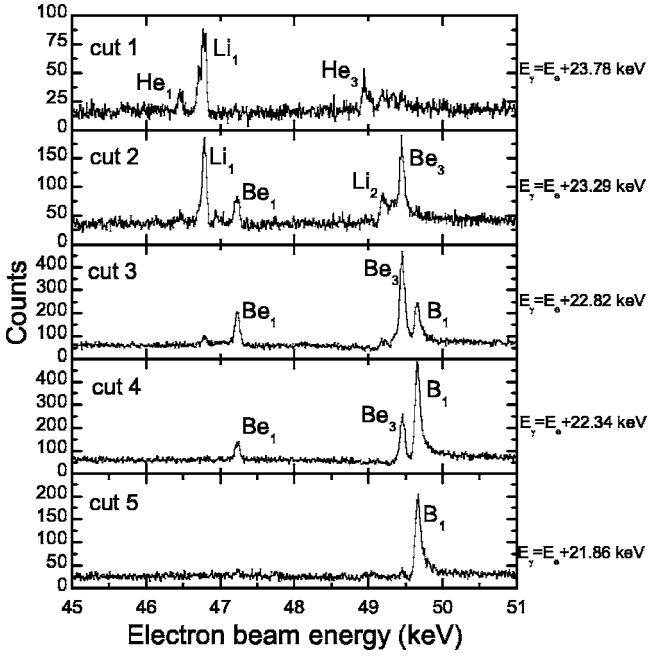

FIG. 4. Projections on the electron energy axis of 480 eV wide slices made along the RR $n=2$, $J=1/2$ band (see the labeled cuts in Fig. 2). On the right side, the variable photon energies E_γ (sum of the electron beam energy E_e and the ionization potential of the corresponding charge state) are indicated in keV.

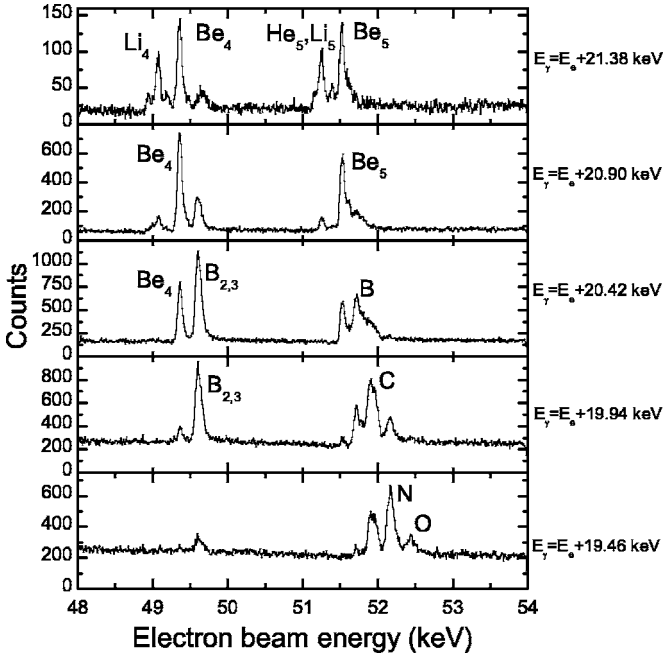

FIG. 5. Projections of the slices along the RR $n=2$, $J=3/2$ band. E_γ and E_e are the photon and electron beam energies in keV, respectively.

closed by white lines in Fig. 2) allow one to study the DR resonances of ions in a specific charge state as the RR photon energies on different slices of each band correspond to different ionization potentials and, thus, ion charge states. Each slice is about 480 eV wide (along the x-ray direction). Typical plots shown in Figs. 4 and 5 correspond to these cuts along the RR $n=2$, $J=1/2$ and $J=3/2$ bands, respectively. The central x-ray energy $E_{\gamma_{\mathrm{RR}}}$ of these slices is roughly equal to $E_{\gamma_{\mathrm{RR}}}=E_e+E_x$, where E_x is chosen as a value close to the ionization potential E_B of ions with a particular charge state. In some cases, the value E_x was shifted from the ionization potential to reduce the influence of strong resonances from the neighboring charge states at the cost of somewhat reduced statistics. For instance, the uppermost slice of the RR ($n=2$, $J=1/2$) band contains DR photons from He-like ions and also a fraction arising from Li-like ions (see Fig. 4, cut 1). In contrast, in cut 3 a strong Be-like ion DR peak (as well as B-like in the $KL_{12}L_3$ region), together with a very weak contribution from a Li-like ion resonance, is observed. The lowest slice, cut 5 of this band, includes almost exclusively DR x rays from B-like ions. The assignment of the observed resonances for a given configuration is based on theoretical energies and strengths for different ion charge states.

To determine the resonance energies, the peaks were fitted with asymmetric Fano profiles [23]. The asymmetry is caused by the interference between DR and RR, as described in detail in Ref. [10]. In a few cases, the resonance profiles could be fitted with pure Gaussian or Lorentzian distributions without loss of accuracy because of their high degree of symmetry (fitting a Gaussian profile to an asymmetric line with a Fano factor of 100 introduces an error of only 0.002% in its resonance position, that is, 1 eV at 50 keV). The weak resonances were also fitted with Gaussian profiles, since the statistical errors in these cases are larger than the shift of the centroid energy induced by the asymmetry as, for instance, in the Be-like resonance Be_1 in cut 4 (Fig. 4). This analysis resulted in an experimental Gaussian width of about 60 eV at 50 keV electron beam energy, corresponding to a relative resolution $\Delta E/E \approx 1/1000$, which is limited mainly by the electron beam energy spread due to the radial gradient of the space charge potential inside the electron beam.

B. DR resonance energies

In order to determine accurately the DR resonance energies, not only the electron acceleration voltage but also the space charge potential due to the dense electron beam have to be precisely known. The total space charge potential of the electron beam (V_{sp}) was estimated using a standard formula [24],

$$V_{\mathrm{sp}}(r=0)[\mathrm{V}] \approx \frac{30 I_e[\mathrm{A}]}{\sqrt{1-\left(\frac{E_e[\mathrm{keV}]}{511}+1\right)^{-2}}}\left[\ln\left(\frac{r_e}{r_{\mathrm{dt}}}\right)^2-1\right]. \quad (1)$$

Equation (1) is given at the center of the electron beam ($r=0$), where r_{dt} and r_e are the radii of the central drift tube electrode (trap) and of the electron beam, respectively. For a 160 mA electron beam current at 46.4 kV acceleration voltage, the electron space charge potential was calculated to be $-(141\pm4)$ eV at the center of the electron beam assuming an electron beam radius of (23 ± 5) μm under our experimental conditions of 8 T. Furthermore, based on other optical spectroscopic measurements, we have estimated (by experience [25–27]) the ion compensation fraction by the accumu-

lated ion charge to be (30±10)% with a conservatively estimated error bar which yields a total effective space charge potential of −99±14 V at 46.4 kV/160 mA.

It is important to estimate the possible change of the space charge compensation when a resonance is hit. Let us assume that a certain charge state contains 40% of the total ion population. As this state is enhancedly recombined at the DR resonance, the population in the next lower charge state increases. This results in a decrease of the ionic charge by the ratio $(q-1)/q$ (where q is the ionic charge), or typically 1.5%, affecting 40% of the ions, at a compensation level of 30%. In this way a 0.2% change of the space charge effects, or roughly 0.2 eV, can be expected at most.

As the space charge potential of the electron beam is inversely proportional to the electron velocity ($E_e^{-1/2}$), the space charge correction obtained for the $1s2s^2$ $KL_{12}L_{12}$ resonance at 46.4 kV was scaled in order to determine the space charge correction for higher and lower electron beam energies. For instance, at the position of the $KL_{12}L_3$ and KL_3L_3 resonances we obtained on average a correction of −97 and −95 V, respectively. The acceleration voltage is constantly monitored. The voltage drifts of the power supplies used, therefore, do not affect the measurement. However, the stability of the voltage divider and of the ADC are essential for these measurements. The electron beam energy spread does not introduce any systematic shift but it broadens the resonance widths.

It is important to emphasize that the scale of the experimental absolute electron energy determined in this way has a systematic error of ±14 eV. This systematic error estimate is mainly due to the contribution of the space charge potential and, by comparison, the uncertainties in the determination of the cathode, drift tubes, and platform voltages are almost negligible (<2 eV). Thus, the present *absolute* DR resonance energy for the $1s2s^2$ state with a nearly symmetric resonance profile [10] was determined to be 46.358 keV ±4 eV (statistical) ±14 eV (systematic), in excellent agreement with all theoretical predictions as shown in Table I. The total uncertainty of the experimental energy scale can be reduced further down to ±4 eV by using as a reference the theoretical value of 46.358 keV obtained for the $1s2s^2$ resonance by multiconfiguration Dirac-Fock ($MCDF_S$) calculations. The DR calculations for He-like ions are expected to be the most reliable among those for many-electron systems and, indeed, show the smallest spread among various models, namely less than 3 eV for the $1s2s^2$ state and around 7 eV for all the other resonances (see Table I). Therefore, using this single theoretical reference, a relative energy scale spanning more than 5 keV (at ≈50 keV) valid for all ionization stages discussed here can be established in addition to the absolute energy scale explained above. As data for all charge states are registered simultaneously, no systematic shifts among them are expected.

Table I compares the experimental results for the charge states ranging from He-like Hg^{78+} to B-like Hg^{75+} ions to calculations carried out with the four theoretical methods described in Sec. II. Figure 6 displays the differences between the experimental and calculated resonance energies. The error bars given in this figure are the relative uncertainties of the experimental data, normalized to the value obtained for the $1s2s^2$ configuration in the respective theoretical approach, as shown in Table I.

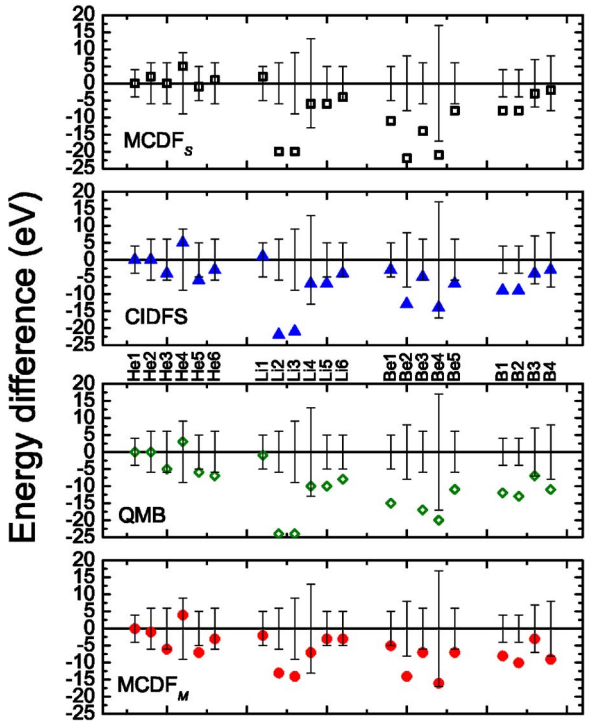

FIG. 6. (Color online) Difference (in eV) between experimental and theoretical results (black open squares for $MCDF_S$, triangles for configuration-interaction Dirac-Fock-Sturm (CI-DFS), rhombus for relativistic many-body perturbation theory (QMB) including first-order QED and second-order relativistic many-body effects, and circles for $MCDF_M$ for the DR resonance energies for capture into He- to B-like mercury ions. Note that in this plot, the experimental energies are referred to the theoretical value of the DR $1s2s^2$ resonance of each individual calculation, in contrast to Table I where the experimental results were pinned to the theoretical value of the $1s2s^2$ $MCDF_S$ calculation. The error bars shown in the plot are those of the relative scale and not those of the absolute one.

It is interesting to note in Fig. 6 that all the predictions have similar tendencies in their deviation from the measured data. Nonetheless, we observe a very good agreement between all the theoretical predictions and the experimental results for the He-like ion DR resonance energies, even for those which are up to 5 keV away from the reference energy. On average, the standard deviation is $\sigma=3$ eV, defined as

$$\sigma = \sqrt{\frac{1}{n}\sum_{i}^{n}(E_{\mathrm{exp,i}} - E_{\mathrm{theo,i}})^2}. \qquad (2)$$

The agreement becomes less satisfactory for the Li-like ion DR resonances. Among these resonances, those for two levels, Li_2 and Li_3 with the same electronic configuration $((1s2s)_1 2p_{1/2})_{3/2} 2p_{3/2}$ but different total angular momenta $J=2$ and $J=1$, respectively, show significant discrepancies reaching $-(20,\ldots,25)$ eV. These differences decrease to −13 eV in the $MCDF_M$ calculations, which include an improved calculation of QED screening effects [13]. A large

TABLE II. Comparison (in keV) between the experimental results and theoretical predictions of the energy separation of DR resonances of few-electron mercury ions. See Table I for the definition of the configurations.

Levels	Experiment	$MCDF_S$	CI-DFS	QMB	$MCDF_M$
He_6-He_1	4.706(6)	4.707	4.702	4.699	4.703
He_6-He_3	2.220(6)	2.221	2.221	2.218	2.223
He_3-He_1	2.486(6)	2.486	2.481	2.481	2.480
He_3-He_5	0.001(6)	0.000	0.000	0.000	0.000
Li_6-Li_1	4.468(4)	4.462	4.463	4.461	4.467
Li_2-Li_3	0.050(9)	0.050	0.050	0.050	0.049
Li_6-Li_2	2.068(6)	2.084	2.085	2.084	2.078
Li_6-Li_4	1.936(12)	1.938	1.942	1.938	1.940
Li_6-Li_5	2.184(4)	2.186	2.186	2.186	2.184
Li_5-Li_1	2.284(4)	2.276	2.277	2.275	2.283
Li_5-Li_4	0.248(12)	0.248	0.244	0.248	0.244
Li_4-Li_1	2.532(12)	2.524	2.521	2.523	2.527
Be_5-Be_1	4.298(5)	4.301	4.294	4.302	4.296
Be_5-Be_3	2.084(6)	2.090	2.082	2.090	2.082
Be_5-Be_4	2.168(17)	2.181	2.175	2.177	2.177
Be_3-Be_4	0.084(17)	0.091	0.093	0.087	0.093
Be_3-Be_1	2.214(5)	2.211	2.212	2.212	2.212
Be_4-Be_1	2.130(16)	2.120	2.119	2.125	2.119
B_4-B_1	2.046(7)	2.052	2.052	2.047	2.045
B_4-B_2	2.104(7)	2.110	2.110	2.106	2.105
B_1-B_2	0.058(1)	0.058	0.058	0.059	0.060
B_1-B_3	0.005(6)	0.000	0.000	0.000	0.000

scatter of about 14 eV among various theories is observed exactly for these resonances (labeled here as Li_2 and Li_3). The result for the Li_5 level, with the same electronic configuration as the Li_2 and Li_3 configurations but with $J=3$, agrees with $MCDF_M$ within a few eV. $MCDF_M$ calculations for the Li-like systems deviate by -7 eV in contrast to the other theoretical methods which are shifted, on average by $-(9,\ldots,13)$ eV.

The measured Be-like ion resonance energies disagree, in general, with all the calculations by $\sigma \approx 9,\ldots,16$ eV. Here, we note that all theories have a pronounced tendency to predict lower values. Nevertheless, it should be noted that the CI-DFS and $MCDF_M$ approaches show a smaller average discrepancy of -8 and -10 eV, respectively, for the Be-like resonances (QMB: ≈ -16 eV). For many cases, the discrepancies are on the level of 2 experimental standard deviations, underlining the need for further experimental and theoretical investigations along the isoelectronic sequences. There is a lesser discrepancy for the B-like ions, with typical deviations of -6 eV for CI-DFS and -5 eV for the $MCDF_S$. A more detailed analysis of the sources of the theoretical uncertainty, including the screening of the Lamb shift, with a detailed breakdown for the various theoretical approaches, will be presented in [13].

C. Difference between energy levels

The differences between the measured resonance energies of specific levels are more accurate because the main systematic errors originating from the determination of the space charge contribution and the acceleration voltage calibration cancel out.

Results for resonance energy differences are shown in Table II and compared to different calculations. Figure 7 displays graphically the deviations compared to the different approaches. The experimental results for different states (with the smallest error bar of 1 eV) are in excellent agreement with all the theoretical predictions. We observe a mean deviation of the $MCDF_M$ predictions from the experimental results of $\sigma=5$ eV (circles in Fig. 7), while that of the CI-DFS calculations (triangles in Fig. 7) slightly increases to 7 eV, both well within the mean experimental error bar of 8 eV.

Only one prediction, the theoretical Li_6-Li_2 value, is about 16 eV higher than the observed result which is well outside the experimental uncertainty. In fact, the energy differences of all other Li resonances with respect to Li_2 or Li_3 disagree significantly with theory, because of the discrepancy in the determination of the excitation energy of the two latter levels, as discussed above (also see Table I). However, the dif-

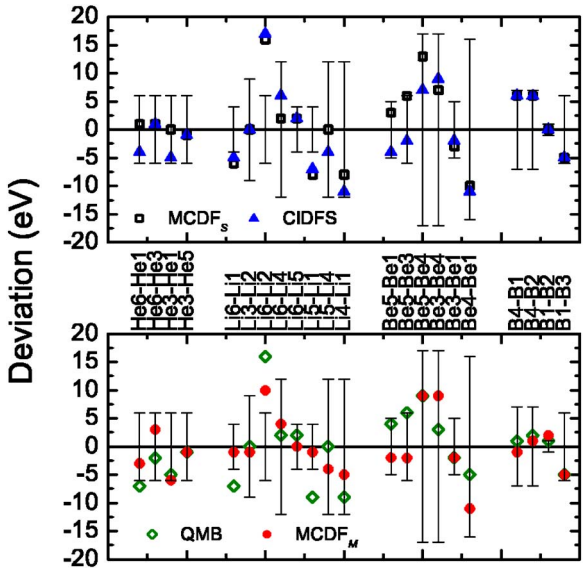

FIG. 7. (Color online) Deviations (in eV) of the various calculations from the present experimental results on the energy separation between DR resonances.

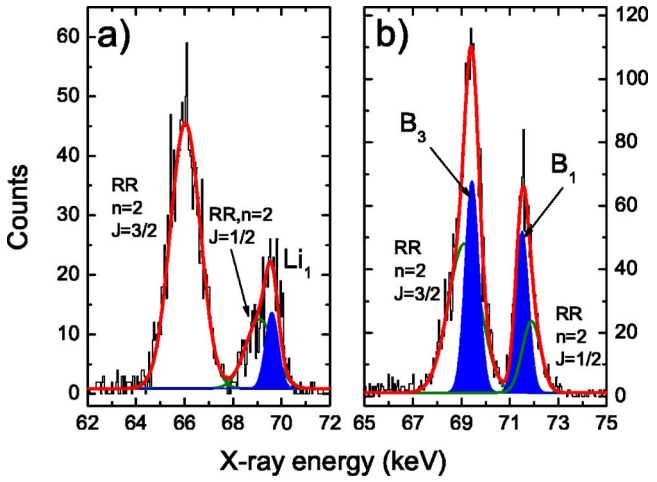

FIG. 8. (Color online) Two projections onto the x-ray axis of a single data set. The two peaks (single lines) always present in these types of projections correspond to the RR $n=2$, $J=1/2$ and $J=3/2$ bands, respectively. (a) Projection of the resonance (filled area) into Li-like states in the $KL_{12}L_{12}$ region. (b) Projection of resonance (filled areas) into B-like states in the $KL_{12}L_3$ region.

ference Li_2-Li_3 agrees well with all the predictions. This comparison shows clearly how essential the treatment of the electron-electron correlation among the different methods is.

V. X-RAY PHOTONS

In addition to the projection of slices along the electron beam axis, we have also performed selective projections onto the x-ray energy axis of the 2D map (Fig. 2) for well-defined windows in the electron energy. At a particular electron beam resonance energy, such projections contain x-ray photons from the DR resonances as well as from RR $n=2$ (two peaks; $J=1/2$ and $J=3/2$, respectively). The RR photon contribution can be extracted from data obtained at nonresonant electron energy values. Since the photon energy of the RR feature depends linearly on the electron beam energy, it is straightforward to estimate its contribution at slightly shifted beam energies. This procedure is performed on both the low and high energy sides of each DR resonance. The width and position of the x-ray signal arising from RR at the DR resonance can be interpolated by these means. In this way, the fitting procedure for the x-ray lines generated by the DR becomes more accurate. Sets of data acquired over 4 h do not allow us to distinguish the small He-like resonances clearly from strong RR x rays. Thus, the highest charge state analyzed here corresponds to Li-like resonances, i.e., Be-like charge states.

As an example, Fig. 8 shows two different projections corresponding to the resonances into Li-like ions in the $KL_{12}L_{12}$ region [Li_1 in Fig. 8(a)] at $E_e=46\,686\pm46$ eV and the resonances into B-like ions labeled B_1 and B_3 in the $KL_{12}L_3$ region [Fig. 8(b)] at $E_e=49\,557\pm61$ eV. The good quality of these fits is inferred from the χ^2/DoF values, which were 0.72 and 0.88 for the spectra containing the Li_1 and B_1 resonances, respectively.

In Fig. 9, the differences between experimental results and the predictions (MCDF$_S$, MCDF$_M$, and QMB) for the measured transitions are plotted (also shown in Table III). It should be pointed out that MCDF$_M$ calculations are carried out for the x-ray energies in the average level approach. Some of the predictions marked with a double subindex have been obtained by averaging a few (two to four) single state values, taking into account their theoretical strengths (e.g., Li_{23} as an average of Li_2 and Li_3). The relatively large error bars ($\approx$60 eV at 72 keV) found in the Li-like ion resonances are due to a low number of counts. Within these uncertainties, a fair agreement with the theoretical predictions is observed. The measured Be-like ion resonance energies, instead, are significantly and consistently smaller than all of the theoretical predictions ($\approx$30 eV), well outside the experimental error bars of ±14 eV. The somewhat larger error bar

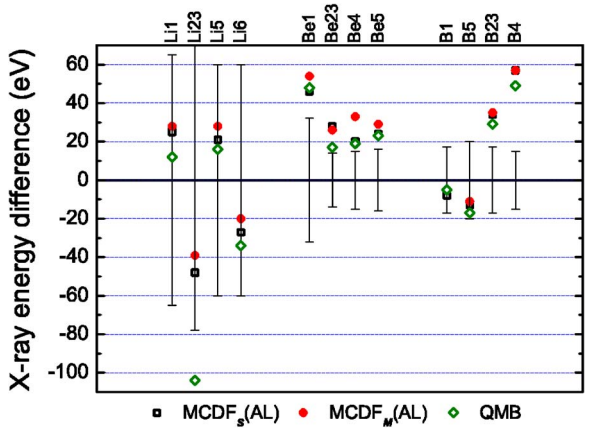

FIG. 9. (Color online) Differences between the observed x-ray energies and the MCDF$_S$ (open squares), the MCDF$_M$ (closed circles), and QMB (open rhombus) calculations. The error bars shown are those of the measured x-ray energies.

TABLE III. Measured x-ray energies (keV) compared with theoretical $MCDF_S$, $MCDF_M$, and QMB calculations for Hg ions in different charge states. The primes accompanying some of the resonance labels indicate the existence of a second resonance, the x-ray energy of which is close to the one under study. Some of the resonances are labeled with two subscripts if two or more single states contribute (see text). $[f]_J$ indicates the final state with its corresponding total angular momentum J.

Label	$[f]_J$	Experiment	$MCDF_S$	$MCDF_M$	QMB
Li_1	$[1s^22s^2]_0$	69.841(65)	69.866	69.869	69.853
Li'_{23}	$[1s^22s2p_{1/2}]_{0,1}$	72.081(78)	72.033	72.042	71.977
Li_5	$[1s^22s2p_{3/2}]_2$	69.805(60)	69.826	69.833	69.821
Li_6	$[1s^22s2p_{3/2}]_2$	72.039(60)	72.012	72.019	72.005
Be_1	$[1s^22s^22p_{1/2}]_{1/2}$	69.657(32)	69.703	69.711	69.705
Be_{23}	$[1s^22s^22p_{1/2}]_{1/2}$	71.879(14)	71.907	71.905	71.896
Be'_4	$[1s^22s^22p_{3/2}]_{3/2}$	69.702(15)	69.722	69.735	69.721
Be_5	$[1s^22s^22p_{3/2}]_{3/2}$	71.880(16)	71.904	71.909	71.903
B_1	$[1s^22s^2(2p_{1/2})^2]_0$	71.674(17)	71.666	71.671	71.669
B_5	$[1s^22s^22p_{1/2}2p_{3/2}]_2$	71.682(20)	71.669	71.669	71.665
B'_{23}	$[1s^22s^22p_{1/2}2p_{3/2}]_{1,2}$	69.551(17)	69.585	69.586	69.580
B_4	$[1s^22s^2(2p_{3/2})^2]_2$	69.546(15)	69.603	69.603	69.595

for the Be_1 resonance is partly due to low statistics and, in addition, to its complete overlap with the RR $n=2$, $J=1/2$ band. Here, the B-like ion resonances at the x-ray energy region around 71.7 keV are found to be in good agreement with the predictions, while the other two resonances at about 69.6 keV are consistently shifted towards lower energies compared to the calculations.

VI. CONCLUSION

In conclusion, the excitation energy of the He-like Hg^{78+} initial state to the Li-like ion $1s2s^2$ resonance at 46.358 keV, resulting in the emission of a photon of 69.678 keV, has been determined with an absolute error bar of ±14 eV. With QED contributions of around 160 eV and nuclear size effects of 50 eV, an accurate test of QED in an average field of 10^{19} V/cm, at a $Z\alpha$ value of $80/137 \approx 0.6$ has been performed. This result nearly reaches the same sensitivity as very recent measurements for the Ly-α transition in hydrogen-like U^{91+} by Gumberidze *et al.* [6], where a precision of ±4.6 eV has been obtained at 100 keV with 250 eV QED and 200 eV nuclear size contributions, respectively.

Our results for the five strongest excitations of the He-like initial ion agree very well, within ±2 eV, with those obtained using four different theoretical methods. This indicates that the calculations are highly reliable for the Li-like excited states. As the energy scale established here is common for the four different charge states being simultaneously observed, a relative energy scale was determined with an uncertainty of ±4 eV.

Deviations of the predictions from our experimental results (in extreme cases as large as 24 eV) have been found for specific resonance states for the Li-, Be-, and B-like initial ions. These discrepancies, in particular, the resonances labeled Li_2 and Li_3 in Table I, also show problems as observed with respect to the scatter of the theoretical predictions. Most likely, these disagreements cannot be attributed to the experimental procedure as they are partly (Be-like systems) found as well in the x-ray channel and in the Fano profiles [10].

Although the x-ray detector resolution limited the accuracy of the x-ray energy measurements, the final results have nonetheless absolute error bars as small as ±14 eV at 70 keV. Thus, they are more accurate than other experiments in *many*-electron high-Z ions, such as the $K\alpha_1$ transitions in U^{90+} ions (100 626±35 eV, Ref. [28]) or in Bi^{81+} (78 825±85 eV, Ref. [29]).

The number of charge states and resonances measured with state selectivity within one scan and otherwise identical experimental setting provides a sensitive tool for the different parts of the calculations, as each state has a different dependence on correlation, QED, and nuclear size effects. A systematic comparison across this isonuclear sequence is therefore a very useful method to benchmark predictions and, in particular, to investigate higher order electron-electron interactions in high fields.

The present QMB calculations neglect some electronic interaction and QED screening contributions and lead to the least satisfactory agreement for configurations with more than three electrons. In principle, only QMB theory offers the possibility of including configuration mixing contributions and *ab initio* QED screening terms in a systematic and exact way. However, the number of these terms and the complexity of the calculation increases factorially with the number of electrons. QMB theory has been successfully applied to the calculation of the low-lying levels of highly charged ions with one to three electrons (see, e.g., [14] and references therein). For the many-electron states, an optimized-level $MCDF_M$ method or the CI-DFS approach reduces the deviations from the experimental data quite substantially (by roughly a factor of 2 as compared to other theoretical approaches).

Further insights on the correlated dynamics of electrons in heavy highly charged ions can be gained by extracting dielectronic resonance strengths from the present experimental data. Results of such an analysis will be the subject of a forthcoming publication.

In order to further reduce systematic errors due to the electron space charge potential, new measurements have been recently carried out with highly charged tungsten ions W^{69+} to W^{72+} ($Z=74$) by varying the electron beam current. The analysis is currently under way. This technique has been applied before for the study of the Ar and Kr *KLL* resonances, and it delivers a directly determined value for the space charge correction. By using electron beam currents as small as possible, an extrapolation to zero current can provide absolute resonance energies with error bars of the order of ±1 eV [19]. The accuracy of the present *absolute* voltage energy scale will be further improved by means of a thermally stabilized high-precision voltage divider developed in the context of this work, which has been recently calibrated at the *Physikalisch-Technische Bundesanstalt*, resulting in a precision of 2.2 V at 220 kV (10 ppm).

ACKNOWLEDGMENTS

A.N.A. and I.I.T. would like to thank the Max-Planck-Institut für Kernphysik (Heidelberg) for the hospitality and perfect work conditions during their stay there. A.N.A. acknowledges financial support of the "Dynasty" foundation. U.D.J. acknowledges support from the Deutsche Forschungsgemeinschaft (Heisenberg program).

[1] H. F. Beyer, H. J. Kluge, and V. P. Shevelko, *X-Ray Radiation of Highly Charged Ions* (Springer, Berlin, 1997).
[2] *Atomic Physics with Heavy Ions*, edited by H. F. Beyer and V. P. Shevelko (Springer, Heidelberg, 1999).
[3] H. F. Beyer and V. P. Shevelko, *Introduction to the Physics of Highly Charged Ions* (IOP, Bristol, 2002).
[4] J. Schweppe *et al.*, Phys. Rev. Lett. **66**, 1434 (1991).
[5] C. Brandau *et al.*, Phys. Rev. Lett. **91**, 073202 (2003).
[6] A. Gumberidze *et al.*, Phys. Rev. Lett. **94**, 223001 (2005).
[7] P. Beiersdorfer, D. Knapp, R. E. Marrs, S. R. Elliott, and M. H. Chen, Phys. Rev. Lett. **71**, 3939 (1993).
[8] P. Beiersdorfer, A. L. Osterheld, J. H. Scofield, J. R. Crespo López-Urrutia, and K. Widmann, Phys. Rev. Lett. **80**, 3022 (1998).
[9] P. Beiersdorfer, H. Chen, D. B. Thorn, and E. Träbert, Phys. Rev. Lett. **95**, 233003 (2005).
[10] A. J. González Martínez *et al.*, Phys. Rev. Lett. **94**, 203201 (2005).
[11] D. A. Knapp, P. Beiersdorfer, M. H. Chen, J. H. Scofield, and D. Schneider, Phys. Rev. Lett. **74**, 54 (1995).
[12] K. G. Dyall, I. P. Grant, C. T. Johnson, F. A. Parpia, and E. P. Plummer, Comput. Phys. Commun. **55**, 425 (1989).
[13] Z. Harman, I. I. Tupitsyn, U. D. Jentschura, C. H. Keitel, A. J. González Martínez, J. R. Crespo López-Urrutia, H. Tawara, and J. Ullrich, Phys. Rev. A **73**, 052711 (2006).
[14] A. N. Artemyev, V. M. Shabaev, V. A. Yerokhin, G. Plunien, and G. Soff, Phys. Rev. A **71**, 062104 (2005).
[15] S. A. Blundell, P. J. Mohr, W. R. Johnson, and J. Sapirstein, Phys. Rev. A **48**, 2615 (1993).
[16] F. A. Parpia, C. F. Fischer, and I. P. Grant, Comput. Phys. Commun. **94**, 249 (1996).
[17] J. R. Crespo López-Urrutia, A. Dorn, R. Moshammer, and J. Ullrich, Phys. Scr., T **80**, 502 (1999).
[18] X. Zhang, J. R. Crespo López-Urrutia, P. Guo, V. Mironov, X. Shi, A. J. González Martínez, H. Tawara, and J. Ullrich, J. Phys. B **37**, 2277 (2004).
[19] A. J. González Martínez, dissertation, Ruperto-Carola University of Heidelberg (2005).
[20] G. W. Drake, G. A. Victor, and A. Dalgrano, Phys. Rev. **180**, 25 (1969).
[21] H. W. Schäffer, R. W. Dunford, E. P. Kanter, S. Cheng, L. J. Curtis, A. E. Livingston, and P. H. Mokler, Phys. Rev. A **59**, 245 (1999).
[22] G. Krake, G. Alber, and J. S. Briggs, J. Phys. B **26**, L561 (1993).
[23] U. Fano, Phys. Rev. **124**, 1866 (1961).
[24] B. E. O'Rourke, dissertation, Department of Pure and Applied Physics, Queen's University of Belfast Northern Ireland (2000).
[25] A. Lapierre *et al.*, Phys. Rev. Lett. **95**, 183001 (2005).
[26] R. Soria Orts, dissertation, Johann Wolfgang Goethe University of Frankfurt am Main (2005).
[27] A preliminary estimate yields a compensation factor of $\approx(42\pm3)\%$ for DR in W^{69+} to W^{72+}, V. Mäckel, private communication, (2005).
[28] J. P. Briand, P. Chevallier, P. Indelicato, K. P. Ziock, and D. Dietrich, Phys. Rev. Lett. **65**, 2761 (1990).
[29] T. Stöhlker *et al.*, Phys. Lett. A **168**, 285 (1992).